

A Gibbs posterior sampler for inverse problem based on prior diffusion model

Jean-François Giovannelli
Groupe Signal-Image, IMS (Univ. Bordeaux, CNRS, BINP), Talence, France

Abstract — This paper addresses the issue of inversion in cases where (1) the observation system is modeled by a linear transformation and additive noise, (2) the problem is ill-posed and regularization is introduced in a Bayesian framework by an a prior density, and (3) the latter is modeled by a diffusion process adjusted on an available large set of examples. In this context, it is known that the issue of posterior sampling is a thorny one. This paper introduces a Gibbs algorithm. It appears that this avenue has not been explored, and we show that this approach is particularly effective and remarkably simple. In addition, it offers a guarantee of convergence in a clearly identified situation. The results are clearly confirmed by numerical simulations.

Index Terms — Inverse problem, deconvolution, Bayesian statistics, Diffusion prior, Learning, MCMC, Gibbs sampler.

I. INTRODUCTION AND PROBLEM FORMULATION

The present paper is devoted to the resolution of inverse problems [1]–[4] when the observation system can be modelled by a linear operator and an additive Gaussian error:

$$\mathbf{y} = \mathbf{H}\mathbf{x}_0 + \mathbf{e}, \quad (1)$$

where \mathbf{x}_0 in \mathbb{R}^P collects the unknowns, \mathbf{y} and \mathbf{e} in \mathbb{R}^M collect the measurements and errors, and \mathbf{H} in $\mathbb{R}^P \times \mathbb{R}^M$ characterizes the operator, *e.g.*, a convolution. The paper focuses on the ill-posed case and the regularization is provided within a Bayesian framework through a prior $\pi_0(\mathbf{x}_0)$. It is considered that a large example set is available, presumed to be made of samples from π_0 .

To describe this prior, a diffusion model is used [5]–[7]: in substance, examples are transformed into noise, and conversely, new examples are generated by transforming noise realizations. To do so, let us define T latent variables $\mathbf{x}_{1:T}$ (in addition to \mathbf{x}_0) and an extended prior $\pi_{0:T}(\mathbf{x}_{0:T})$. In order to define the latter, let us introduce two joint pdfs for $\mathbf{x}_{0:T}$: a *forward* denoted $p_{0:T}^+$ and a *backward* denoted $p_{0:T}^-$. For practical efficiency, both are chosen in Markovian form:

$$p_{0:T}^+(\mathbf{x}_{0:T}) = p_0^+(\mathbf{x}_0) \prod_{t=1}^T p_{t|t-1}^+(\mathbf{x}_t | \mathbf{x}_{t-1}) \quad (2)$$

$$p_{0:T}^-(\mathbf{x}_{0:T}) = p_T^-(\mathbf{x}_T) \prod_{t=0}^{T-1} p_{t|t+1}^-(\mathbf{x}_t | \mathbf{x}_{t+1}) \quad (3)$$

which reveals two terminal marginal pdfs p_0^+ and p_T^- and two sets of transition pdfs $p_{t|t-1}^+$ and $p_{t|t+1}^-$. Regarding the terminals

$$\begin{aligned} p_0^+(\mathbf{x}_0) &= \pi_0(\mathbf{x}_0) \\ p_T^-(\mathbf{x}_T) &= \mathcal{N}(\mathbf{x}_T; \mathbf{0}, \mathbf{I}) \end{aligned}$$

the first is the pdf π_0 of the example set and the second is the pdf of noise (Gaussian, white, zero-mean, unitary variance).

With regard to transitions, again for practical efficiency, Gaussians are chosen with the following parameters.

$$p_{t|t-1}^+(\mathbf{x}_t | \mathbf{x}_{t-1}) = \mathcal{N}(\mathbf{x}_t; k_t \mathbf{x}_{t-1}, v_t^+ \mathbf{I}) \quad (4)$$

$$p_{t|t+1}^-(\mathbf{x}_t | \mathbf{x}_{t+1}) = \mathcal{N}(\mathbf{x}_t; \mu_t(\mathbf{x}_{t+1}), v_t^- \mathbf{I}) \quad (5)$$

The function $\mu_t(\mathbf{x})$ can be seen as a *denoiser* and it is described by a neural network $\mu_t^\theta(\mathbf{x})$, with parameter θ . It has two inputs: the image \mathbf{x} (to be denoised) and the time t providing information on the levels of noise v_t^+ and attenuation k_t . Replacing μ_t by μ_t^θ in (5), and substituting in (3), yields $p_{t|t+1}^{-,\theta}$ and $p_{0:T}^{-,\theta}$. Regarding the hyperparameters k_t , v_t^+ , v_t^- we refer to the usual Variance Preserving scheme [5]–[7].

The learning stage adjusts θ to minimise the Kullback distance between the forward $p_{0:T}^+$ and backward $p_{0:T}^{-,\theta}$ pdfs

$$\mathcal{D}[p_{0:T}^+; p_{0:T}^{-,\theta}]$$

while ensuring that the marginal pdfs for \mathbf{x}_0 and \mathbf{x}_T are

$$\begin{cases} \pi_0 & \simeq p_0^+ \simeq p_0^- \\ \mathcal{N} & \simeq p_T^- \simeq p_T^+ \end{cases}$$

i.e., that of the example set and the noise. It suffices then to report the adjusted value of θ in $\mu_t^\theta(\mathbf{x})$ and $p_{0:T}^{-,\theta}$ to obtain an adjusted joint backward pdf (3). Based on its Markov and Gauss structure, it is then easy to sample:

$$\mathbf{x}_T \sim \mathcal{N}(\cdot; \mathbf{0}, \mathbf{I})$$

$$\mathbf{x}_t \sim \mathcal{N}(\mathbf{x}_t; \mu_t^\theta(\mathbf{x}_{t+1}), v_t^- \mathbf{I}), \quad \text{for } t = T-1, \dots, 1, 0.$$

Start by drawing an image \mathbf{x}_T as a noise. Then, repeat the following two steps, from $t = T-1$ to $t = 0$:

- pass the image through the network $\mu_t^\theta(\mathbf{x}_{t+1})$ and
- add white noise with zero-mean and variance v_t^- .

It is referred to as *ancestral sampling*. The results are particularly convincing and it is now a standard practice to seek to use this pdf and sampler in the Bayesian inversion.

To do so, the measurements are included *via* the likelihood deduced from the observation model (1) and a model for the error. Here the latter is described as zero-mean and white with variance v_e , so $f(\mathbf{y}|\mathbf{x}_0) = \mathcal{N}(\mathbf{y}; \mathbf{H}\mathbf{x}_0, v_e \mathbf{I})$. We can then construct the extended joint pdf $f(\mathbf{y}, \mathbf{x}_{0:T}) = f(\mathbf{y}|\mathbf{x}_0) \pi_{0:T}(\mathbf{x}_{0:T})$ and the extended posterior:

$$\pi_{0:T}(\mathbf{x}_{0:T} | \mathbf{y}) = \frac{f(\mathbf{y}, \mathbf{x}_{0:T})}{f(\mathbf{y})} = \frac{f(\mathbf{y}|\mathbf{x}_0) \pi_{0:T}(\mathbf{x}_{0:T})}{f(\mathbf{y})}.$$

$$\mathbf{y} \text{ --- } \mathbf{x}_0 \text{ --- } \mathbf{x}_1 \text{ --- } \mathbf{x}_2 \text{ --- } \cdots \text{ --- } \mathbf{x}_{t-1} \text{ --- } \mathbf{x}_t \text{ --- } \mathbf{x}_{t+1} \text{ --- } \cdots \text{ --- } \mathbf{x}_{T-1} \text{ --- } \mathbf{x}_T$$

Fig. 1. Hierarchy: \mathbf{x}_0 is the image of interest, $\mathbf{x}_{1:T}$ are the latent images and \mathbf{y} is the measured image (blurred and noisy version of the true \mathbf{x}_0).

This development is based on a model with a natural conditional independence property: the pdfs for $(\mathbf{y}|\mathbf{x}_0)$ and $(\mathbf{y}|\mathbf{x}_{0:T})$ are equal (see the hierarchical representation in Fig. 1).

II. SAMPLING: EXISTING APPROACHES AND LIMITATIONS

The main difficulty is then to sample from the posterior in our specific context of a prior based on a diffusion model.

In recent years, there have been a number of papers devoted to this issue. [8] and [9] respectively introduce Diffusion Posterior Sampling (DPS) and Pseudoinverse-guided Diffusion Models (II-GDM). They rely on the likelihood attached to \mathbf{x}_t (instead of \mathbf{x}_0) and on an approximation based on Tweedie's formula. [10] introduces the Twisted Diffusion Sampler (TDS): a SMC (Sequential Monte Carlo) algorithm targets the posterior, based on a set of weighted particles. [11] proposes an idea inherited from Bayesian filtering: Filtering Posterior Sampling (FPS) that introduces latent measurements. An extended version also leverages SMC methods. [12] proposes Diffusion Posterior MCMC (DPMC) based on Annealed MCMC, *i.e.*, defines a series of intermediate pdfs. [13] defines a sequence of intermediate linear inverse problems, then also a sequence of pdfs that are sampled from by means of SMC. [14] introduces variable splitting to divide the sampling task into two simpler steps: a linear-Gauss one (Wiener/Tikhonov) and a denoising one carried out by the diffusion model. [15] offers a comprehensive overview of MC methods and an analysis of the idea of twisting in relation with other approaches.

Some methods are resolutely approximate [8], [9], while others aim to target the posterior [10]–[13]. The latter are essentially based on the concept of SMC and their convergence is for large enough number of particles. In any case, they all appear to be inspired by the idea of ancestral sampling, in that each image \mathbf{x}_t is visited once, and in the direction from $t = T$ to $t = 0$. However, while ancestral sampling is certainly attractive for the prior, it is not effective for the posterior.

III. PROPOSED SAMPLER: A GIBBS SCHEME

The paper now presents the contribution: a Gibbs algorithm for the joint posterior $\pi_{0:T}(\mathbf{x}_{0:T}|\mathbf{y})$. It samples each \mathbf{x}_t in turn¹, under its conditional pdf $\pi_{t|\star}(\mathbf{x}_t|\mathbf{y}, \mathbf{x}_{t|\star})$ where $(t|\star)$ is the set of times from 0 to T except t itself.

The approach taken here aims to obtain a direct algorithm, in the sense that these conditionals can be sampled directly, typically a Gauss. The original idea is to play with both forward and backward pdfs (switch to play, say). More specifically, the sampling is based on the posterior attached to the

- forward $\pi_{0:T}^+(\mathbf{x}_{0:T}|\mathbf{y})$ for the latent variables $\mathbf{x}_{1:T}$, and
- backward $\pi_{0:T}^-(\mathbf{x}_{0:T}|\mathbf{y})$ for the object of interest \mathbf{x}_0 .

¹This is actually a Block-Gibbs version (each image \mathbf{x}_t constituting a block), but we will simply refer to it as Gibbs for the sake of simplicity.

This idea is justified by the fact that the two joint priors $\pi_{0:T}^+(\mathbf{x}_{0:T})$ and $\pi_{0:T}^-(\mathbf{x}_{0:T})$ are similar thanks to the learning stage, and we consider here they are identical. Work is ongoing to account for the fact that they are not strictly identical.

1 - Image of interest — Regarding \mathbf{x}_0 , it is sampled under $\pi_{0|\star}(\mathbf{x}_0|\mathbf{y}, \mathbf{x}_{0|\star})$ and given the hierarchy (Fig. 1)

$$\begin{aligned} \pi_{0|\star}(\mathbf{x}_0|\mathbf{y}, \mathbf{x}_{0|\star}) \\ \propto p_{0|1}^-(\mathbf{x}_0|\mathbf{x}_1) f(\mathbf{y}|\mathbf{x}_0) \\ = \mathcal{N}(\mathbf{x}_0; \boldsymbol{\mu}_0(\mathbf{x}_1), v_0^- \mathbf{I}) \mathcal{N}(\mathbf{y}; \mathbf{H}\mathbf{x}_0, v_e \mathbf{I}) \end{aligned}$$

which reveals a linear-Gauss problem. The co-logarithm² reads

$$\begin{aligned} \text{colog } \pi_{0|\star}(\mathbf{x}_0|\mathbf{y}, \mathbf{x}_{0|\star}) \\ \# \|\mathbf{x}_0 - \boldsymbol{\mu}_0(\mathbf{x}_1)\|^2 / v_0^- + \|\mathbf{y} - \mathbf{H}\mathbf{x}_0\|^2 / v_e. \end{aligned}$$

So, the conditional posterior is Gauss with precision and expectation (involving the classic Wiener/Tikhonov solution).

$$\begin{cases} \boldsymbol{\Gamma}_0 &= \mathbf{H}^t \mathbf{H} / v_e + \mathbf{I} / v_0^- \\ \boldsymbol{\varepsilon}_0 &= \boldsymbol{\Gamma}_0^{-1} (\mathbf{H}^t \mathbf{y} / v_e + \boldsymbol{\mu}_0(\mathbf{x}_1) / v_0^-) \end{cases}$$

Sampling is particularly effective in the Fourier plane: the components are independent and Gaussian, and their mean and variance are easily obtained by simple FFT [16].

2.1 - Latent images ($t \neq T$) — The case of $\mathbf{x}_{1:T}$ also rely on the hierarchy (Fig. 1). Naturally, it is needed to separate the termination $t = T$ from the other t . For $t = 1, \dots, T-1$

$$\begin{aligned} \pi_{t|\star}(\mathbf{x}_t|\mathbf{y}, \mathbf{x}_{t|\star}) \\ \propto p_{t|t-1}^+(\mathbf{x}_t|\mathbf{x}_{t-1}) p_{t+1|t}^+(\mathbf{x}_{t+1}|\mathbf{x}_t) \\ = \mathcal{N}(\mathbf{x}_t; k_t \mathbf{x}_{t-1}, v_t^+ \mathbf{I}) \mathcal{N}(\mathbf{x}_{t+1}; k_{t+1} \mathbf{x}_t, v_{t+1}^+ \mathbf{I}) \end{aligned}$$

so, by writing the co-logarithm²

$$\begin{aligned} \text{colog } \pi_{t|\star}(\mathbf{x}_t|\mathbf{y}, \mathbf{x}_{t|\star}) \\ \# \|\mathbf{x}_t - k_t \mathbf{x}_{t-1}\|^2 / v_t^+ + \|\mathbf{x}_{t+1} - k_{t+1} \mathbf{x}_t\|^2 / v_{t+1}^+ \end{aligned}$$

a Gauss pdf is identified with precision $\gamma_t \mathbf{I}$ and expectation $\boldsymbol{\varepsilon}_t$

$$\begin{cases} \gamma_t &= 1/v_t^+ + k_{t+1}^2/v_{t+1}^+ \\ \boldsymbol{\varepsilon}_t &= \gamma_t^{-1} (k_t \mathbf{x}_{t-1} / v_t^+ + k_{t+1} \mathbf{x}_{t+1} / v_{t+1}^+) \end{cases}$$

2.2 - Latent image ($t = T$) — For the case of \mathbf{x}_T , based on the hierarchy (Fig. 1):

$$\begin{aligned} \pi_{T|\star}(\mathbf{x}_T|\mathbf{y}, \mathbf{x}_{T|\star}) &= p_{T|T-1}^+(\mathbf{x}_T|\mathbf{x}_{T-1}) \\ &= \mathcal{N}(\mathbf{x}_T; k_T \mathbf{x}_{T-1}, v_T^+ \mathbf{I}) \end{aligned}$$

²to within one term and a factor of 2

i.e., simply the last step in the forward process: a Gaussian with precision $\gamma_T \mathbf{I}$ and expectation $\boldsymbol{\varepsilon}_T$

$$\begin{cases} \gamma_T = 1/v_T^+ \\ \boldsymbol{\varepsilon}_T = k_T \boldsymbol{x}_{T-1} \end{cases}$$

Overall, the entire algorithm is both simple and efficient.

- First, this requires the sampling of Gaussians only.
- Second, all the covariances are diagonal be it in the Fourier domain ($t = 0$) or in the spatial one ($t \neq 0$).
- In addition, means and variances are easy to compute, by FFT ($t = 0$) or linear combination ($t \neq 0$).

It is called G-DPS for Gibbs-Diffusion Posterior Sampling.

Convergence property — A crucial point is that the Gibbs scheme is guaranteed to converge (for large enough number of iterations). It provides samples under the joint pdf by sampling the conditional pdfs (deduced from the joint pdf). However, strictly speaking, the result does not apply here since some conditionals are deduced from the forward (joint) pdf and others from the backward (joint) pdf. That said, by its nature, the learning stage brings the forward and backward pdfs close together, so it is considered that guarantee is provided. Work is ongoing to obtain a full convergence guarantee.

IV. NUMERICAL ASSESSMENT

A. Simulation details

In order to demonstrate the feasibility and interest of the proposed G-DPS, an experimental study is proposed. It relies on a toy problem based on the MNIST example set. The method has been implemented within the computing environment Matlab³ and the information regarding the architecture and learning stage are given in [18]. For a first experiment: the ground-truth \boldsymbol{x}^* is a sample of the learned prior (size 32×32 , gray level roughly in $[0, 1]$), the PSF is a 3×3 square, and the noise level is $\sigma_e = 0.05$. The ground-truth \boldsymbol{x}^* and the measurement \boldsymbol{y} , i.e., blurred and noisy image, are shown in Fig. 4 (left and middle).

Here are some points regarding implementation details.

- The image \boldsymbol{x}_0 is initialized to \boldsymbol{y} . The $\boldsymbol{x}_{1:T}$ are set to successive noisy versions through the forward scheme.
- Regarding the scan order: the algorithm update the images for $t = 0, 1, \dots$ up to $t = T$ and repeats this pattern.
- As iterations proceed, the empirical average of images is updated. The algorithm stops when the difference between successive updates is smaller than a threshold.

Remark — The algorithm has been run numerous times, under identical and different scenarios (ground-truth, noise level, PSF and initializations): it has always shown consistent qualitative and quantitative behaviours and we have never detected any convergence or numerical instability issues.

B. Results

Fig. 2 shows a typical result regarding three pixels. A standard behaviour is observed for the chains: the distributions

³on a standard PC with a 3.8 GHz CPU (Intel(R) Core(TM) i7-10700K) and 32 GB of RAM, and a GPU...

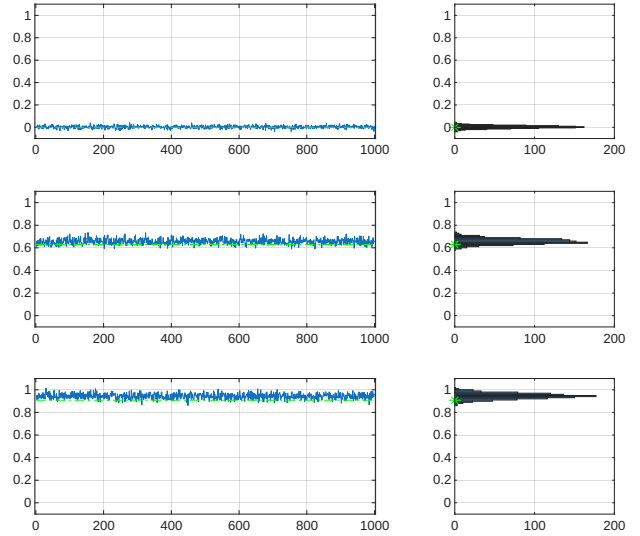


Fig. 2. Samples provided by the Gibbs algorithm for three pixels of \boldsymbol{x}_0 . They are shown as a function of iteration index (left) and as histograms (right). They are samples of one dimensional marginal pdfs. See also Fig. 3 and Tab. I. The green lines/dots give the true value.

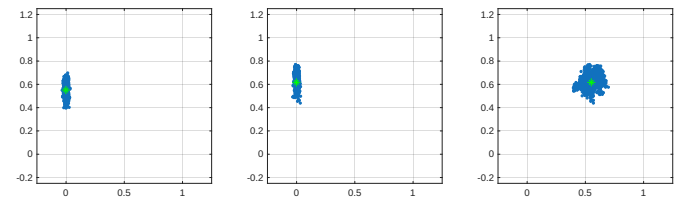


Fig. 3. Point clouds for two dimensional marginals pdfs for three pixels. The sample are given in blue and the true value is given in green. See also Fig. 2 for one dimensional plots and Tab. I for quantitative assessment.

quickly stabilise and seem stationary after about only 10 iterations (burn-in period). From a qualitative view, Fig. 2 shows that the estimated gray levels are nearby the ground-truth (known in this simulation study). The quantitative results are reported in Tab. I.

	Pixel 1	Pixel 2	Pixel 3
True	-0.00142	0.55092	0.61704
Estimate	0.00122	0.61773	0.69163
Error	0.0026	0.0668	0.0746
PSD	0.01020	0.05730	0.05719
$\pm 2\text{PSD}$	✓	✓	✓

TABLE I

Results for three pixels: true and estimated values (first and second row) then the error (third row). The Posterior Standard Deviation (PSD) is then given and the ✓ indicates that the true value does lie within the interval with center the estimate and width two PSD. See also Figs. 2 and 3.

Finally, Fig. 4-right yield the estimated image. The blur and the noise are significantly reduced in the resulting image (Fig. 4-right) with respect to the measurement (Fig. 4-middle) and it closely matches the original image (Fig. 4-left). This result is confirmed by the cross-sections also in presented in Fig. 4 and by the quantitative results in Tab. I.

As a Bayesian and sampling one, the proposed strategy

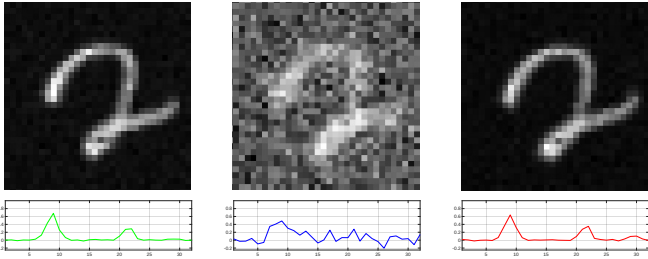


Fig. 4. Left to right: true object \mathbf{x}^* , measurements \mathbf{y} and estimated object $\hat{\mathbf{x}}$. The figure shows the images themselves (top) and cross-sections (bottom).

provides not only optimal estimation for the unknowns (e.g., Posterior Mean as the MMSE), but also coherent tool for uncertainty quantification. More specifically, sampling the posterior enable to compute (a) estimation and (b) posterior standard deviations (PSD) as empirical averages based on the samples. From Fig. 5 and Tab. I it is clear that, for each pixel, the true value lies within the interval of center the estimate and of width two standard deviations. This reinforces the relevance of the Bayesian strategy and the importance of the quality of posterior sampling for the correct quantification of uncertainty.

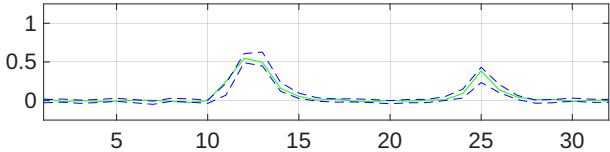


Fig. 5. Cross-sections of \mathbf{x}^* (plain green) and the “uncertainty” intervals (dashed blue) with center the estimate and of width two standard deviations.

C. Additional consideration regarding convergence

This section explores the issue of speed of convergence in greater depth, from an empirical perspective. The left-hand side of Fig. 6 shows the convergence of the empirical average of the samples (for the three considered pixels) towards its limit (the posterior mean⁴). The figure shows effective convergence: as for the first pixel, convergence is essentially instantaneous, whereas for the other two pixels, it seems to take effect after approximately 300 iterations.

The right-hand side of Fig. 6 shows the correlation of the chain for each of the three pixels (correlation across iterations). For the first one, the correlation drops almost immediately to 0, which is consistent with the fact that the empirical average converges very quickly. For the other two pixels, it decreases less rapidly, and we can approximately consider that beyond 250 iterations, the correlation is slight. This decrease is also consistent, qualitatively, with the convergence of the empirical average, which is slower than for the first pixel.

D. Efficiency, computation time and some comments

The algorithm produces N samples $\mathbf{x}_{0:T}^{(n)}$ for $n = 1, \dots, N$ under the joint pdf for $\mathbf{x}_{0:T}$. The images of interest $\mathbf{x}_0^{(n)}$ are obtained by simple projective marginalisation, *i.e.*, discarding

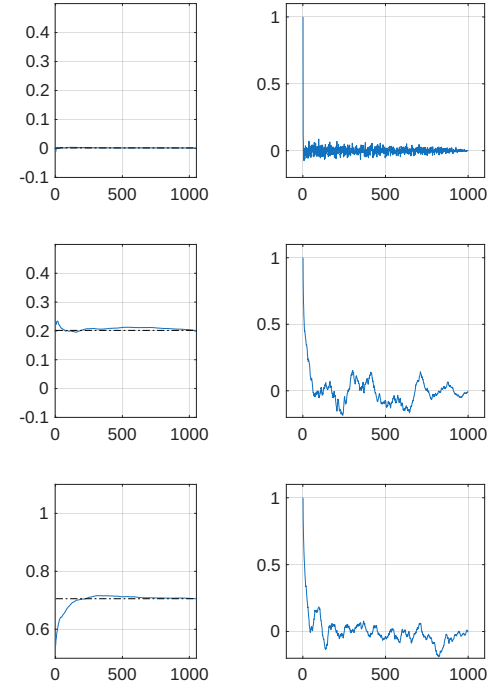


Fig. 6. Left part: empirical average of the samples provided by the Gibbs algorithm as a function of iteration index n for three pixels of \mathbf{x}_0 . Right part: correlation of the chain (across the iterations of the Gibbs algorithm). Comments are given in Sect IV-C.

the $\mathbf{x}_{1:T}^{(n)}$. It should be noted that an iteration n includes updating all images (for $t = 0, \dots, T$).

As mentioned earlier, as iterations progress, the empirical average of the images $\mathbf{x}_0^{(n)}$ (approximating the posterior mean⁴) is updated. The iterations stops when the difference between successive updates becomes smaller than a threshold, practically set to 10^{-2} . The algorithm thus iterated $N = 1030$ times which took 53 seconds. Most of the calculation time (about 85%) is due to the passage through the network.

A particular feature of the G-DPS sampling scheme is that, ultimately, each iteration n requires only a single pass through the neural network (to update $\mathbf{x}_0^{(n)}$). Thus, scaling up to larger images does not appear to be an obstacle.

Furthermore, for the proposed G-DSP algorithm, as for many others, it is possible to take advantage of parallelisation in the “batch” direction in order to simulate several independent samples in parallel. This possibility is supported by GPU architectures and most programming languages (Python, Matlab, etc.). We therefore have significant potential gains in terms of computing time.

Another major practical advantage of G-DSP is that it does not require the adjustment of any algorithm parameters or fine-tuning quantities (apart from the number of iterations), unlike many other algorithms.

⁴Considering that the guarantee of convergence of the sampler to the posterior is provided (see *Convergence property* at the end of Sect. III).

V. CONCLUSION: G-DSP AN ATTRACTIVE ALGORITHM

This paper deals with numerical methods for solving inverse problems when the observation model is linear with additive Gauss noise. Developments are within a Bayesian framework: it provides optimal estimates and uncertainty quantification. The prior is founded on a diffusion model adjusted on a large set of examples. Posterior sampling is a challenging question, and we propose a new answer.

More precisely, we turn towards a Gibbs loop that splits the overall problem in far simpler sub-problems: iteratively sample each image under its conditional posterior. These conditionals are all Gaussian and their moments are easily calculated (using the backward form for the image of interest and the forward form for the latent variables). It seems that this idea has not been explored in the literature for this context (diffusion prior and inverse problem). This is possibly due to the fact that the community has focused on ideas inspired by the ancestral sampling with the intent to correct / guide its behaviour.

A crucial point is that of the convergence guarantee. Although this guarantee does not rigorously exist (since G-PDS relies partly on the forward density and partly on the backward density), it is certainly possible to refer to a form of guarantee since the forward and backward densities are similar at the end of the learning stage.

The simulation study focuses on the issue of image deconvolution and is based on the MNIST example set. It demonstrates that the algorithm correctly samples the posterior distribution. Therefore, it provides accurate and coherent elements for uncertainty quantification, as well as accurate image restoration. This numerical study also confirms the remarkable computational efficiency.

Conclusively, the proposed paper addresses the crucial question of sampling the posterior in an inverse problem based on a diffusion prior and it provides an original, proper and highly efficient answer.

To go further, it would be interesting to include the estimation of additional parameters *e.g.*, noise level (hyperparameter estimation, automatic adjustment, self-tuned...) [19] or instrument parameters [16], [20], [21] (myopic, self-calibrated, semi-blind...) when some observation system parameters are also unknown. This question is partly addressed in [22].

Another perspective is to evaluate the performance of G-DPS in comparison to others, based for example on [23], [24].

ACKNOWLEDGMENT

The author warmly thanks Liam Moroy, Guillaume Bourmaud, Frédéric Champagnat, Marcelo Pereyra and Charlesquin Kemajou for their help.

This work is conducted within project *PEPR Origins*, reference ANR-22-EXOR-0016, supported by the France 2030 plan managed by Agence Nationale de la Recherche. It also received financial support from the French government in the framework of the University of Bordeaux's France 2030 program / RRI ORIGINS.

REFERENCES

- [1] J.-F. Giovannelli and J. Idier, Eds., *Regularization and Bayesian Methods for Inverse Problems in Signal and Image Processing*. London: ISTE and John Wiley & Sons Inc., 2015.
- [2] J. Kaipio and E. Somersalo, *Statistical and computational inverse problems*. Berlin, Germany: Springer, 2005.
- [3] J. C. Santamarina and D. Fratta, *Discrete Signals and Inverse Problems: An Introduction for Engineers and Scientists*. Chichester, England: WileyBlackwell, 2005.
- [4] P. C. Hansen, *Discrete Inverse Problems: Insight and Algorithms*. Philadelphia, USA: Society for Industrial and Applied Mathematics, 2010.
- [5] S. H. Chan, *Tutorial on Diffusion Models for Imaging and Vision*, ser. Foundations and Trends in Machine Learning. Hanover, MA, USA: Now Publishers Inc, Jan. 2024.
- [6] F. D. S. Ribeiro and B. Glocker, *Demystifying Variational Diffusion Models*, ser. Foundations and Trends in Machine Learning. Hanover, MA, USA: Now Publishers Inc, Jan. 2025.
- [7] P. Nakkiran, A. Bradley, and M. Zhou, Hattieand Advani, *Step-by-Step Diffusion: An Elementary Tutorial*, ser. Foundations and Trends in Machine Learning. Hanover, MA, USA: Now Publishers Inc, 2025.
- [8] H. Chung, J. Kim, M. T. McCann, M. L. Klasky, and J. C. Ye, "Diffusion posterior sampling for general noisy inverse problems," 2024.
- [9] J. Song, A. Vahdat, M. Mardani, and J. Kautz, "Pseudoinverse-guided diffusion models for inverse problems," in *International Conference on Learning Representations*, 2023.
- [10] L. Wu, B. Trippe, C. Naesseth, D. Blei, and J. P. Cunningham, "Practical and asymptotically exact conditional sampling in diffusion models," in *Advances in Neural Information Processing Systems*, vol. 36, 2023, pp. 31372–31403.
- [11] Z. Dou and Y. Song, "Diffusion posterior sampling for linear inverse problem solving: A filtering perspective," in *The 12-th International Conference on Learning Representations*, Vienna, Austria, May 2024.
- [12] Y. Zhu, Z. Dou, H. Zheng, Y. Zhang, Y. N. Wu, and R. Gao, "Think twice before you act: Improving inverse problem solving with MCMC," 2024. [Online]. Available: <https://arxiv.org/abs/2409.08551>
- [13] G. Cardoso, Y. Janati, S. Le Corff, and E. Moulines, "Monte Carlo guided diffusion for Bayesian linear inverse problems," 2023. [Online]. Available: <https://arxiv.org/abs/2308.07983>
- [14] F. Coeurdoux, N. Dobigeon, and P. Chainais, "Plug-and-play split Gibbs sampler: Embedding deep generative priors in Bayesian inference," *IEEE Trans. Image Processing*, vol. 33, pp. 3496–3507, 2024.
- [15] Y. Janati, E. Moulines, J. Olsson, and A. Oliviero-Durmus, "Bridging diffusion posterior sampling and Monte Carlo methods: a survey," *Philosophical Transactions of the Royal Society A*, vol. 383, no. 2299, 2025. [Online]. Available: <https://doi.org/10.1098/rsta.2024.0331>
- [16] F. Orieux, J.-F. Giovannelli, and T. Rodet, "Bayesian estimation of regularization and point spread function parameters for Wiener-Hunt deconvolution," *J. Opt. Soc. Amer.*, vol. 27, no. 7, pp. 1593–1607, July 2010.
- [17] N. Yismaw, U. S. Kamilov, and M. S. Asif, "Gaussian is all you need: A unified framework for solving inverse problems via diffusion posterior sampling," *IEEE Trans. Computational Imaging*, vol. 11, pp. 1020–1030, 2025.
- [18] MatlabDoc (fr.mathworks.com/help/), "Generate images using diffusion," [deeplearning/ug/generate-images-using-diffusion.html](https://fr.mathworks.com/help/deeplearning/ug/generate-images-using-diffusion.html), 2023.
- [19] F. Orieux, J.-F. Giovannelli, T. Rodet, H. Ayasso, M. Husson, and A. Abergel, "Super-resolution in map-making based on a physical instrument model and regularized inversion. Application to SPIRE/Herschel," *Astron. Astrophys.*, vol. 539, Mar. 2012.
- [20] C. Vacar, J.-F. Giovannelli, and Y. Berthoumieu, "Bayesian texture and instrument parameter estimation from blurred and noisy images using MCMC," *IEEE Signal Proc. Let.*, vol. 21, no. 6, pp. 707–711, 2014.
- [21] P. Campisi and E. K., Eds., *Blind Image Deconvolution*. CRC Press, 2007.
- [22] J.-F. Giovannelli, "Estimation of instrument and noise parameters for inverse problem based on prior diffusion model," *submitted to Proc. IEEE ICIP*, Sep. 2026.
- [23] L. Moroy, G. Bourmaud, F. Champagnat, and J.-F. Giovannelli, "Evaluating the posterior sampling ability of Plug&Play diffusion methods in sparse-view CT," in *Proc. IEEE ICASSP*, Hyderabad, India, Apr. 2025.

[24] ——, “On the posterior gap in plug & play diffusion methods for sparse-view computed tomography,” *IEEE Journal of Selected Topics in Signal Processing*, Jan. 2026.